Technical Report

Development of Technologies of NSSC STH™2 Thick Steel Plate for Hydrogen Use

Masaharu HATANO* Mitsuki SUGEOI
Yoichi YAMAMOTO Tatsumi HAMADA

Abstract

In this paper, hydrogen embrittlement of a new stainless steel, STH2, has been examined with respect to the effects of TIG welded joints, the fracture resistance and hydrogen embrittlement resistance at low temperature technologies for liquid hydrogen use. TIG welded joints using STH2 co-metal showed a high Charpy absorption energy of 0.2% PS, about twice that of SUS316L, in liquid hydrogen (−253°C). Prestrain at −196°C and Charpy impact tests showed high fracture resistance due to the suppression of γ→α′ transformation, and fracture resistance was maintained even when about 30 ppm hydrogen was charged. The increase of 0.2% PS at low temperatures of STH2 is considered to be due to changes in the dislocation structure due to a decrease in γ_{SFE}. In addition, it is presumed that STH2 exhibited good fracture resistance properties as a result of suppressed localization of stress concentration due to the excessive development of planar dislocation sequences.

1. Introduction

Presently, for a high pressure hydrogen gas environment, the use of SUS316L (17.5Cr-12–14Ni-2Mo) is exemplified and standardized.[1, 2] SUS316L is a representative high corrosion resistant stainless steel[3] with high contents of rare metals such as Ni and Mo, and 0.2% proof stress (hereafter referred to as 0.2%PS) which is used as the standard in structural design and is relatively low. To date, we have developed N-added low Ni and Mo-saving type stainless steel (hereafter referred to as STH2[*1]) as a new material for hydrogen material replacing SUS316L.[4–7]

In the alloy design of STH2, in order to obtain hydrogen embrittlement resistance at −40°C under 70 MPaH_2, against the basic compositions of 15Cr-9Mn steel, with the addition of Ni and N etc., Ni equivalent was determined according to Sanga's equation.

Ni+0.72Cr+0.88Mo+1.11Mn-0.27Si+0.53Cu+12.93C+7.55N≥30.2

The hydrogen embrittlement resistance is in good agreement with the stability of the austenite (γ) phase expressed by Sanga's equation[8], and the STH2 steel plate actually produced (Ni equivalent 30.5) is equipped with high strength and suitability for the high pressure hydrogen gas environment.[7] Recently, as the application technology of STH2 steel plate to fuel cell battery vehicles, we reported hydrogen embrittlement resistance when TIG welding or a high cold reduction ratio of higher than 70% is applied.[9]

As for the expansion of hydrogen utilization, in addition to the target of 3 million tons/year in 2030 under the updated Basic Hydrogen Strategy (revised in June, 2023) by the Japanese Government, a target of introducing 12 million tons/year in 2040 was raised. In the Basic Strategy, a scheme of producing liquid hydrogen in great quantities in the countries having rich primary energy resources, and transporting such produced gas by tankers to harbors in the regions of concentrated industry in Japan has been prepared. At that time, large low temperature storage tanks like that of LNG currently in service were set as the core equipment.[10]

Against such a background, to promote the application of STH2 to liquid hydrogen, Nippon Steel Stainless Steel Corporation manufactured STH2 steel plate on an actual production line. As the application technology of the STH2 thick steel plate so manufactured on an actual line to liquid hydrogen, this paper describes the result of the evaluation of the properties of TIG welded joints, low temperature fracture resistance properties, and the low temperature hydrogen embrittlement resistance properties.

[*1] STH denotes a trademark. STH: Stainless Steel with Twinning Induced Plasticity for Hydrogen Energy Systems

* Dr.Eng., Senior Chief Researcher, New Energy Material Research & Development Div., Research & Development Center, Nippon Steel Stainless Steel Corporation
3434 Ooaza-shimata, Hikari City, Yamaguchi Pref. 743-8550

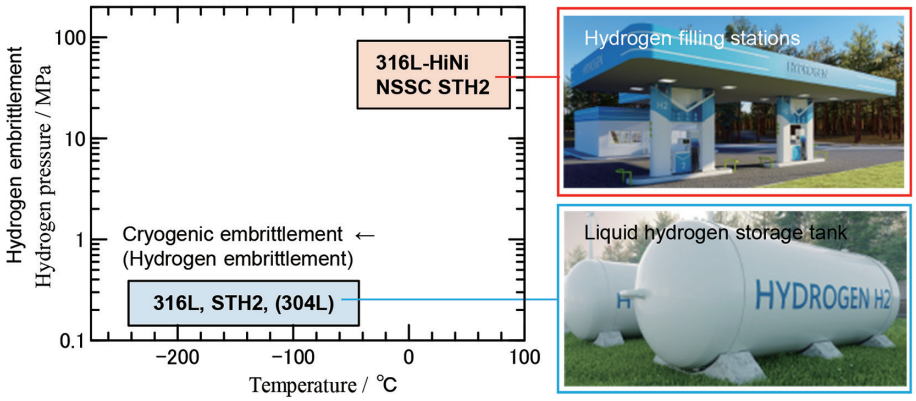

Fig. 1 Nippon Steel Stainless Steel Corporation (NSSC) recommended materials and application examples for hydrogen environments

2. Recommended Material for Application to Liquid Hydrogen

SUS304L and/or SUS316L are readily available on the market as general-use stainless steel, and are representative materials for liquid hydrogen used for storage tanks, transportation containers, and pipings.[11] Not only the base metals, but also the welded joints of these stainless steels exhibit high toughness even under the cryogenic environment of −253°C of liquid hydrogen.[12]

Since in the liquid hydrogen storage tank, the part above the liquid level and the piping are exposed to the low temperature gaseous hydrogen atmosphere, it is necessary to take into account the occurrence of deterioration of fracture properties due to hydrogen gas embrittlement in the gaseous phase. In the past, hydrogen penetration of 7.5 ppm to the depth of 2 mm was reported in the exposure test under 10 MPaH_2 at 100°C based on the assumption that the liquid hydrogen storage tank undergoes long-term service during which period inspection and/or heat-up are carried out.[13] As for the base metals and the welded joints of SUS304L and SUS316L, it has also been clarified that the hydrogen charge of about 10 ppm does not exert any influence on the fracture properties.[12, 13] Furthermore, hydrogen gas embrittlement in a low temperature region is evaluated for various austenitic stainless steels by the slow strain rate tensile test (SSRT) in 1 MPaH_2.[11, 14] Hydrogen gas embrittlement of austenitic stainless steels becomes highest around −40 to −80°C, and decreases as the temperature lowers, and disappears at around −150°C. Since SUS304L has high susceptibility to hydrogen gas embrittlement at −40 to −80°C, the use of SUS316L is recommended when the hydrogen gas embrittlement in a low temperature region is taken into account.

Figure 1 shows the materials recommended by Nippon Steel Stainless Steel and their application examples for hydrogen environments based on the hydrogen or cryogenic embrittlement. For the high pressure hydrogen gaseous environment represented by that of a hydrogen station, STH2 (Ni equivalent 30.5) is recommended in addition to SUS316L-HiNi (17.5Cr-13.5Ni-2Mo) which conforms to the exemplified standard. Under the cryogenic environment represented by that of the liquid hydrogen storage tank, SUS304L (18Cr-9Ni) and/or SUS316L (17.5Cr-12Ni-2Mo) have been used. When hydrogen gas embrittlement in a low temperature region is considered, application of SUS316L or STH2 is desirable. STH2 having hydrogen gas embrittlement resistance is a potent recommended material to replace SUS316L even under the cryogenic environment.

Table 1 NSSC recommended material standards

NSSC standard JIS standard	Main chemical compositions / %	Ni_{eq} 1)	0.2%PS MPa	TS MPa	EL %
NSSC STH2	15Cr-9Mn-Ni+N	30.5	≥ 275	≥ 550	≥ 40
SUS316L-HiNi	18Cr-13.5Ni-2.2Mo	30.4	≥ 175	≥ 480	≥ 40
SUS316L	18Cr-12Ni-2.1Mo	28.0			
SUS304L	18Cr-9Ni	24.5			

1) Ni_{eq} = Ni+0.72Cr+0.88Mo+1.11Mn-0.27Si+12.93C+0.53Cu+7.55N

Table 1 shows the recommended material standards. STH2 conforms to the NSSC independent standard of Nippon Steel Stainless Steel, and the abovementioned three steel grades conform to the JIS standard (JIS G 4303). Ni equivalent was sought from the chemical compositions of the practically applied representative material, and by using Sanga's equation. STH2 is characterized by high strength with the addition of N, and as compared with the other three steel grades, 0.2%PS and the tensile strength (hereafter referred to as TS) exceed by about 1.5 times and 1.1 times, respectively. Elongation (hereafter referred to as EL) of STH2 is equivalent to those of the other three steel grades under the solution treatment state, the standard value of which is equal to or above 40%. In view of the recent growth in the scale of liquid hydrogen storage tanks, study on the application of STH2 is significant from the viewpoints of resource-saving, reduction of cost by using thinner material, and improvement in welding workability.

3. Experiment Method

3.1 Evaluation of TIG welded joint properties

Test pieces were taken from the actually produced STH2 thick steel plate of 20 mm, applied with annealing and pickling after hot rolling from a cast slab. TIG welded joint samples assumed for liquid storage tanks were prepared by two pieces of a 20 mm thick × 200 mm wide × 600 mm long STH2 thick steel plate as one set, and by welding the length of about 600 mm. As the filler metal, a 1.2 mm square bar cut out from a 1.2 mm thick STH2 steel sheet[7] was used. **Table 2** shows the welding condition of the TIG welded joints, and **Fig. 2** shows the schematic illustrations of the TIG welded joint bevel shapes and fused depositions. The welding condition was: heat input: 13.2 kJ/cm; feeding rate of filler metal: 7 to 10 g/mm; shielding gas: 100%Ar, and the fused deposit was laminated keeping the interlamination temperature difference below 150°C. Two types of beveling of V shape and レ shape were arranged, and the

former was used for the tensile test of the weld metal and the welded joint, and the latter was used for the Charpy test.

The tensile test was applied to the thick steel plate, weld metal, and the welded joints at room temperature, conforming to JIS Z 2241. The tensile tests in liquid nitrogen (−196°C) and in liquid hydrogen (−253°C) were applied to the thick steel plate and welded joints. Tensile test pieces of smooth round bars of 6 mmΦ and 7 mmΦ at the respective parallel section were taken at t/2 in the C axis direction. Gauge length was 30 mm and 25 mm, respectively. The strain rate in the nitrogen liquid was 5.0×10^{-5}/s until the strain reaches 0.2%PS, and 6.6×10^{-4}/s afterwards, and in the case of liquid hydrogen, 5.0×10^{-4}/s until 0.2%PS is reached, and 1.0×10^{-3}/s afterwards. The Charpy test conformed to JIS Z 2242, and was carried out at −196°C, using liquid nitrogen, and at −253°C using liquid He. The Charpy test piece was a 2 mm V-notched test piece of JIS No.4, and the test pieces were taken at the t/2 of the thick steel plate in the rolling direction and in the traverse direction to welding. Charpy absorption energy and the lateral expansion were measured, and the fracture surface was observed by SEM.

3.2 Evaluation of fracture resistance properties and hydrogen embrittlement resistance properties at low temperature

The fracture resistance properties of STH2 thick steel plate were evaluated by combining the tensile prestrain and the Charpy impact test at −196°C. Tabular tensile test pieces (gauge length 50 mm) of 5 mm in thickness were taken in the longitudinal direction at the t/2 of a 20 mm thick steel plate. The prestrain at −196°C was provided within the cross head displacement range of 2.5 to 10 mm in liquid nitrogen, and the elongation due to prestrain was measured after the test. The tensioning rate was controlled to 1.2 mm/min by cross head control, and the volume ratio of ferrite (volume ratio of α') of the material prestrained at −196°C was measured by a ferrite meter. Charpy sub-size test pieces of 2 mm V-notch were taken from the parallel section of the prestrained material, and underwent a Charpy test at −196°C, and the fracture surface was observed by SEM. Furthermore, the dislocation microstructure was observed by a transmission electron microscope JEM-F200 at the acceleration voltage of 200 kV.

Hydrogen embrittlement resistance properties were evaluated by the low temperature toughness of hydrogen-charged material in addition to SSRT at −40°C under 1 $MPaH_2$. For SSRT, round bar test pieces 3 mmΦ × 20 mm in length at the parallel section were taken from t/2 of a 20 mm thick steel plate, and the test was carried out at a strain rate of 10^{-5}/s under 1 $MPaH_2$ and 0.1 $MPaN_2$ at −40°C. Hydrogen charging[15] was conducted under the condition of 300°C × 10 $MPaH_2$ × 96 h which enables charging at 30 ppm[13] of hydrogen, larger than the one in actual usage, evenly within the plate thickness of 2 mm in a short time. Volume and the present state of hydrogen were measured with thermal desorption analysis (hereafter referred to as TDA). Low temperature toughness of the hydrogen-charged material was evaluated by the Charpy impact value at −196°C, and the fracture surface was observed by SEM. Furthermore, for comparison purposes, a material heat treated in open air at 300°C for 96 h was prepared, and the Charpy test and analysis of an extracted TEM replica were conducted.

Table 2 Welding conditions of TIG welded joint

Current A	Voltage V	Speed cm/min	Heat input kJ/cm	Wire feeding rate, g/min	Shielding gas L/min
200	11	10	13.2	7–10	Ar, 25

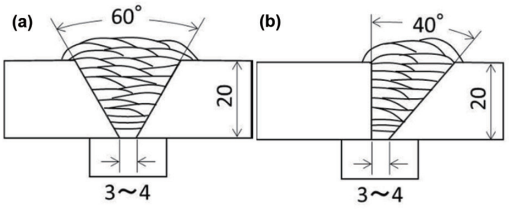

Fig. 2 Schematic illustration of TIG welded joint bevel shapes and fused depositions

4. Result and Study

4.1 Result of evaluation of TIG welded joint properties

In the TIG welded joints, defects such as lack of joint penetration and/or cracks were not found, and the weld workability was no different to that of the general-use steel of SUS316L. Furthermore, the welded joints were inspected by radiographic examination (JIS Z 3106), and were confirmed free of blow holes or the like, and the result was provided for evaluation of the properties.

Figure 3 shows the representative cross-sectional microscope images of the welded joint. The observation was made as to: (a) base metal, (b) weld metal, and (c) fusion line near the center of the plate thickness. The base metal is of the γ single phase microstructure including the twin crystal developed by annealing, and the crystal grain size is about GS No.6 of (JIS G 0551). The weld metal consists of only the original γ phase which grew to columnar form, and

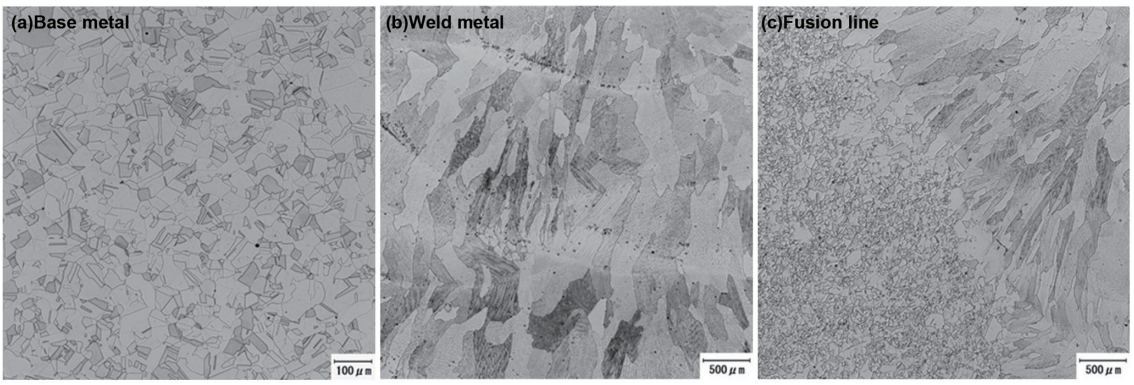

Fig. 3 Optical microscope images of 20 mm thick plate base metal and welded joint

δ ferrite is not observed. The volume of ferrite is not detected by the ferrite meter, which does not contradict the observation result of the microstructure. At the fusion line, microstructure consists of the columnar crystal γ phase observed in the weld metal and the γ phase of the base metal, and coarsening of the crystal grain is not observed. From the above, it is confirmed that TIG welded joints using the filler metal of STH2 do not produce δ ferrite, and that the microstructure consists of only the γ single phase.

Table 3 shows the tensile properties of a TIG welded joint. Tensile test pieces are: JIS No.4 (base metal), JIS No.A2 (weld metal), and JIS No.1A (welded joint). In the tensile tests, tension was applied to the base metal and the welded joint test pieces in the parallel direction for the rolling direction (RD), and in the traverse direction (TD) for the welded joints. 0.2%PS and TS of the weld metal are higher than those of the base metal, and the fracture of the welded joint took place at the base metal. The increase of the strength of the weld metal having a grain size larger than that of the base metal is attributed to the effect of the welding residual stress caused by the plastic constraint. Fracture elongation of the base metal is 60%, and is high, exceeding 40% even in the case of the weld metal. Thus, TIG welded joints using the filler metal of STH2 have realized high strength and high ductility at room temperature, exceeding the level of the base metal where fracture took place.

Figure 4 shows the tensile properties of the base metals and welded joints in liquid hydrogen (−253°C), liquid nitrogen (−196°C), and at room temperature. At each temperature, the two values (n=2) of those of the base metal and welded joint is plotted. 0.2%PS and TS increase significantly below −196°C. The base metal strength increases by 2.0 to 3.2 times, and the welded joint strength increases by 1.6 to 2.0 times higher vs. the strength at room temperature. Particularly, the base metal exhibits 0.2%PS exceeding 1 000 MPa and TS exceeding 1 500 MPa at −253°C, and the value of 0.2%PS is about two times higher than that of SUS316L[12]. The strength of the welded joint was equivalent to the base metal at −196°C and about 90% of the base metal at −253°C due to fracture at the weld metal, but the strength was maintained at a sufficiently high level (about 1.8 times higher) than that of SUS316L. In the past, it was found that 0.2%PS and TS of the type 316 austenitic stainless steel increase with the increase of the N content in the range of 0.05 to 0.17%.[16] The increase of the strength of the base metal and the welded joint of STH2 is similar in behavior to those of the type 316 austenitic stainless steel added with 0.17% N and the one added with 0.12% N,[16] and the influence of the content of N is considered to be the main cause. Thus, STH2 exhibits 0.2%PS about two times higher than that of SUS316L at −196 to −253°C both at the base metal and welded joint, and it has been pointed out that strength increases with the addition of N.

Table 3 Tensile properties of TIG welded joint

	Tensile test piece	0.2%PS MPa	TS MPa	EL %	Fracture
Base metal	JIS No.4, RD	338	663	60.0	-
Weld metal	JIS No.A2, RD	526	700	43.3	-
Welded joint	JIS No.1A, TD		671		Base metal

The Charpy absorption energy of the base metal and welded joints at −253°C and −196°C is shown in **Fig. 5**. Each of the Charpy absorption energies of the base metal, weld metal, and the fusion line is the average of two (n=2). The Charpy absorption energy at −196°C and at −253°C do not show temperature dependency, and are almost equal, and the values of the base metal are high and exceed 200 J. Although the Charpy absorption energy drops to about 100 J in the weld metal and the fusion line, the values are still higher than that of the absorption energy of SUS316L obtained in the past WE-NET (World Energy Network: International Clean Energy System Technology Utilizing Hydrogen).[12, 13] The factor which deteriorates the toughness of the weld metal is considered to be δ ferrite and inclusions (carbide, oxide). The Charpy absorption energy in the cryogenic environment of the weld metal of the type 316 is reported to be expressed by the prediction formula (i)[13]. Since STH2 weld metal did not produce δ ferrite, and maintained carbon and oxygen in the same volume ratio as that of the base metal, it is interpreted that Charpy absorption energy higher than that of SUS316L has been achieved.

$$vE\ (J) = 90.6 - 4.56\ (FN) - 44.2\ (\%C) - 824\ (\%O) \qquad (i)$$

FN: Ferrite number of the filler metal

%C, %O: volume ratios of carbon, oxygen

Figure 6 shows the relationship between the Charpy absorption energy at −253°C and the lateral expansion. The Charpy absorption energy shows a linear relation with respect to the increase of lateral expansion as found in the past.[13] In the design of a pressure vessel conforming to JIS B 8267, the minimum lateral expansion is specified to be 0.4 mm. The lateral expansion of the STH2 weld metal and the fusion line exceeds 0.9 mm, and exhibits a value sufficiently

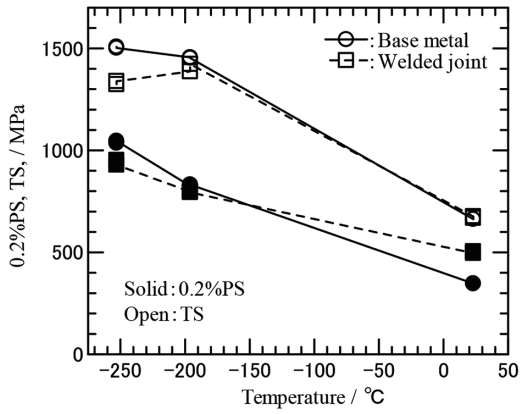

Fig. 4 Tensile properties of base metals and welded joints in cryogenic refrigerants and at room temperature

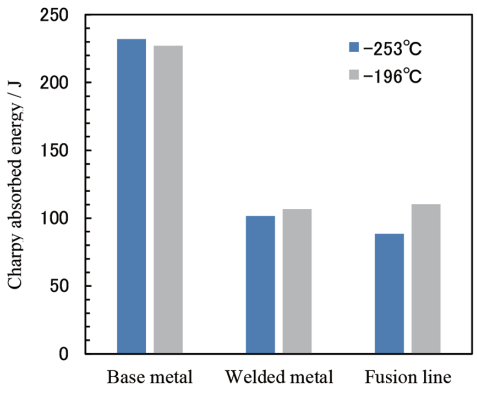

Fig. 5 Charpy absorption energy of base metal and welded joints at −253°C and −196°C

high for practical use. SEM photos of the fracture surfaces of Charpy test pieces at −253°C are shown in **Fig. 7**. The fracture surface of the base metal exhibits a dimple pattern developed by ductile fracture. The weld metal exhibits a fracture surface configuration with ups and downs larger than those of the base metal, which exhibits a dimple pattern when the fracture photo is enlarged. In the weld metal of SUS316L which includes δ ferrite, fractures and/or cracks alongside δ ferrite are observable;[13] however, such microcracks are not confirmed in the STH2 weld metal.

Thus, in liquid hydrogen, the TIG welded joint using STH2 filler metal exhibits 0.2%PS about two times higher than that of the one of SUS316L and high Charpy absorption energy, and therefore STH2 is recommended as the prospective material to replace SUS316L in the cryogenic environment.

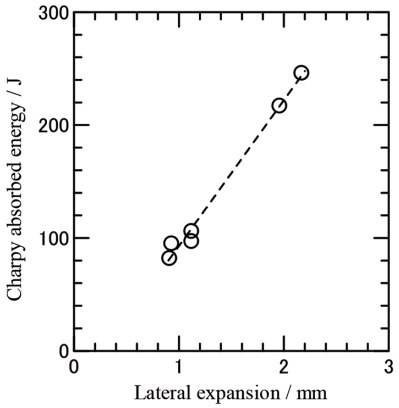

Fig. 6 Relationship between Charpy absorption energy at −253°C and lateral expansion

4.2 Result of evaluation of fracture resistance properties and hydrogen embrittlement resistance properties at low temperature

For the clarification of fracture resistance properties of liquid hydrogen storage tanks, the influence of deformation-induced martensite (α') formed in the austenitic stainless steels at low temperatures needs to be considered. According to a past report, the volume ratio of formed α' of SUS316L does not change in the tensile test between −256°C and −196°C.[11] Then, fracture resistance properties of the STH2 thick steel plate were evaluated by combining the tensile prestrain and Charpy impact test at −196°C. The results are shown in **Fig. 8**. The stress of the prestrained material at −196°C increases in the range of 770 to 1 120 MPa by the displacement of the cross head from 2.5 to 10 mm. The measured values of elongation are in the range of 0.2 to 12.4%, and the volume ratio of α' of these prestrained materials is less than 2% even when the elongation is 12.4%. In the case of below −196°C, the volume ratio of α' of

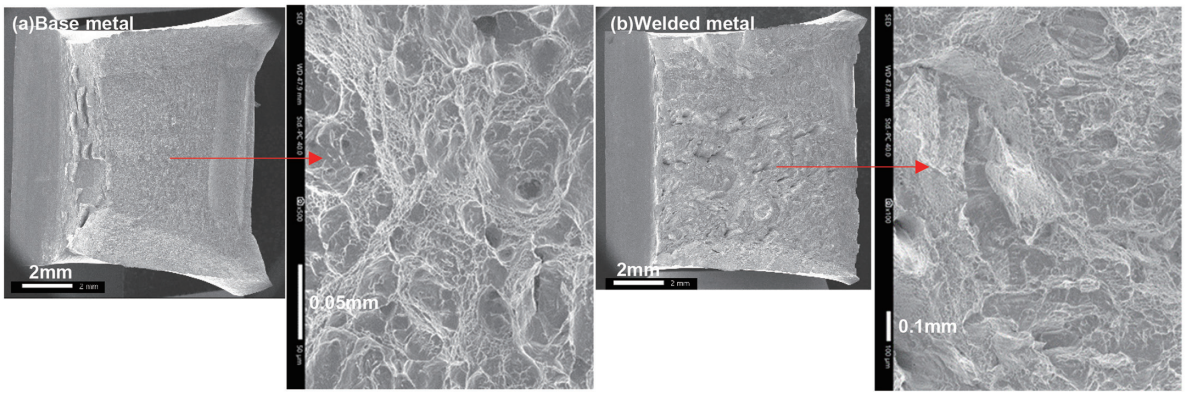

Fig. 7 SEM observation results of fracture surface of base metal and welded metal at −253°C

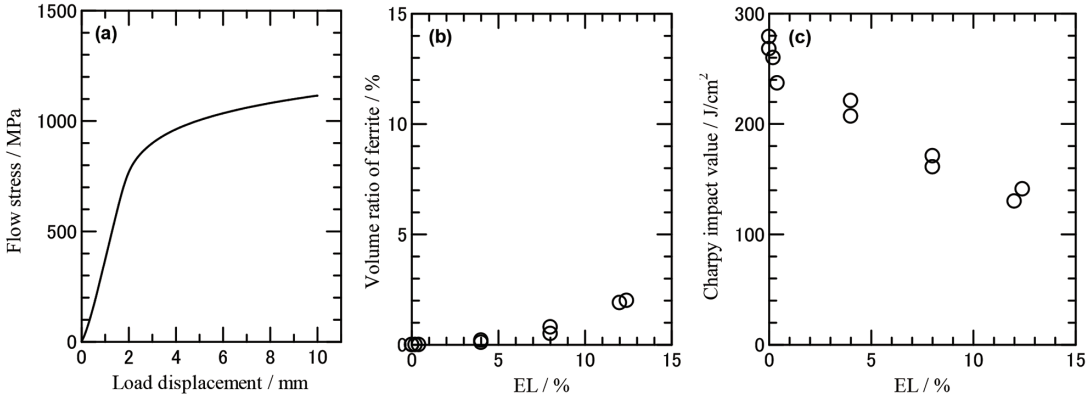

Fig. 8 Effect of prestrain at −196°C on cryo-fracture properties
(a) Stress-displacement curve of a prestrain specimen at −196°C (b) Volume ratio of ferrite of prestrain specimens at −196°C (c) Charpy impact value at −196°C

SUS316L increases to about 10% in the neighborhood of elongation of 10%.[11] $\gamma \rightarrow \alpha'$ transformation of STH2 has been suppressed more greatly than in the case of SUS316L. Charpy impact values deteriorate due to plastic deformation of elongation of 4.0 to 12.4%; however, they exceed greatly the guideline for the ductile fracture of materials for LNG tanks (EN1460-2 standard > 60 J/cm^2). **Figure 9** shows the fracture surface of a Charpy test piece of a 12.4% prestrained material (provided with 1 120 MPa). After the Charpy test, plastic deformation due to lateral expansion is observed, and the fracture surface exhibits a ductile fracture surface with a dimple pattern. The above indicates that STH2 thick steel plate exhibits excellent fracture resistance properties owing to the suppression of $\gamma \rightarrow \alpha'$ transformation by prestrain and the Charpy impact test at −196°C.

Figure 10 shows the result of observation by TEM of the dislocation microstructure of 0.4% prestrained material (770 MPa provided) which clarifies the γ phase deformation elementary process prestrained at −196°C. An electron beam was injected into <110> as shown in (a), and the bright-field image of the dislocation microstructure was photographed. As shown in (b), dislocation scatters within on the sliding surface of {111}, consisting of linear type ones, and curved and partly intertwined type ones. As observable in the enlarged view (c), the linear type dislocation shows stacking faults formed by the expansion of partial dislocation. These stacking faults formed in the early stage of deformation are understood to be attributed to the deterioration of stacking fault energy (γ_{SFE}) below −196°C. In the high nitrogen stainless steels having low γ_{SFE}, formation and the development of planar dislocation array formed into a line are reported to increase yielding strength and work-hardenability ratio.[17] The increase of 0.2%PS and TS of STH2 at low temperatures is considered to be attributed to the change of the dislocation microstructure of the γ phase due to deterioration of γ_{SFE}. Additionally, STH2 is presumed to express the aforementioned excellent fracture resistance properties as a result of the suppression of the localization of stress concentration due to excessive development of planar dislocation array.

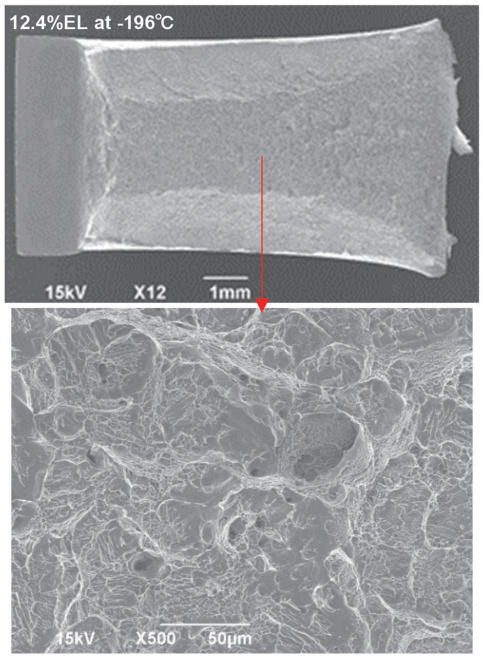

Fig. 9 SEM observation results of fracture surface of a prestrain specimen at −196°C

Hydrogen gas embrittlement resistance at low temperatures obtained the SSRT properties at −40°C under 1 MPa hydrogen, conducted by WE-NET/PJ. Hydrogen suitability was evaluated, taking as an indicator, the new criterion of elongation specified in the revised General Gas Security Regulation[2]. SSRT properties in gaseous hydrogen of 1 MPa at −40°C of STH2 and SUS304L thick steel plates are shown in **Fig. 11**. In 1 MPaH_2, STH2 exhibits 0.2%PS 1.5 times higher than that of SUS304L, and high elongation exceeding 60%. Relative tensile strength (RTS) and relative elongation (REL) to values standardized for 0.1 MPaN_2 are 1.0 and 0.95 to 1.03, respectively. The new criterion means that the elongation under the influence of gaseous hydrogen satisfies the standard, and from the result, elongation is estimated as (1), (2), and (3), wherein the material elongation values are those obtained through tensile tests conducted at room temperature.

STH2-1: 60% (material elongation) × 1.0 (REL) = 60% (1)
STH2-2: 61% (material elongation) × 0.95 (REL) = 58% (2)
SUS304L: 62% (material elongation) × 0.59 (REL) = 37% (3)

Elongation of STH2 is 60% and 58%, and largely exceeds 40% of the recommended material standards (Table 1). In the meantime,

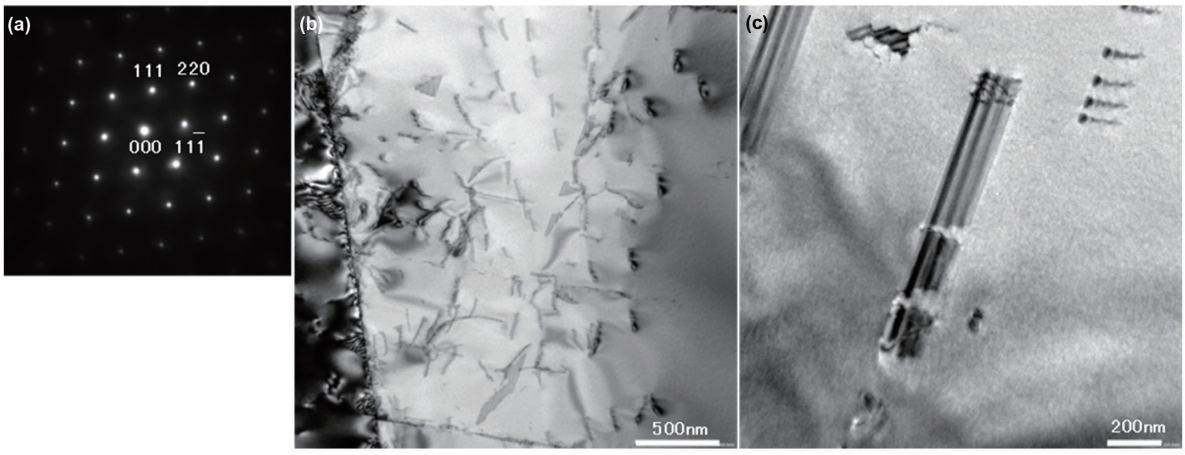

Fig. 10 Dislocation microstructure of the specimen after 0.4% deformation at −196°C
(a) Electron diffraction pattern from <110>$_{fcc}$ reflection (b) Bright-field image of dislocation configurations (c) Bright-field image of stacking faults

elongation of SUS304L is 37%, and is known not to reach 40% of the recommended material (Table 1). Thus, STH2 thick steel plate exhibits hydrogen suitability under low temperature gaseous hydrogen.

Low temperature fracture resistance properties with the influence of hydrogen being taken into consideration were evaluated by the Charpy impact test at −196°C with hydrogen charged by 30 ppm which is three times higher than that expected in a liquid hydrogen storage tank[13]. Results obtained from 2 mm thick steel plates of STH2 and 316L-HiNi are shown in **Fig. 12**. The volume of hydrogen measured with TDA is STH2: 32.5 ppm, and 316L-HiNi: 28.0 ppm, and the targeted volume of hydrogen was successfully charged. Hydrogen desorption spectrums reach peak at 450°C, and exhibit a single form, and hydrogen is almost desorbed below 600°C. A past article reports that the desorption rate of diffusive hydrogen of austenitic stainless steels reaches its peak at 450°C, and the peak appears at 600°C in the case of non-diffusive hydrogen.[13] From the result, the charged hydrogen is categorized as diffusive hydrogen.

The Charpy impact value at −196°C shows the average of two values (n=2). Charpy impact values are in the range of 140 to 150 J/cm^2, and greatly exceed the guideline for the ductile fracture (EN1460-2 standard > 60 J/cm^2), and do not deteriorate even when hydrogen of 30 ppm is absorbed and held inside. From the SEM observation of the fractured surface, as opposed to the fracture configuration of the dimple pattern of STH2, in the case of 316L-HiNi, scattering internal cracks initiating at the center of the plate thickness as shown by white arrows are found. The above indicates that STH2 maintains excellent low temperature fracture resistance properties even when it has absorbed and is held inside about 30 ppm hydrogen.

Past SUS316L paper reports the deterioration of Charpy energy absorption and the occurrence of internal cracks due to hydrogen charging at 400 to 600°C, and the influence of the change in microstructure due to thermal hysteresis is pointed out as the cause.[13] In this experiment, in order to eliminate the influence of thermal hysteresis to the extent possible, the temperature was limited to lower than 300°C. In 316L-HiNi, although deterioration of the Charpy impact value is not recognized, internal cracks occurred near the center of the plate thickness. **Figure 13** shows results of the examination of the precipitation behavior for the heat treatment of 300°C × 96 h based on the analysis of the extracted replica TEM. From the TEM image, regions wherein minute precipitates under 50 nm in particle size and with an interparticle range of less than 1 μm exist are found scattered here and there. It is known that, from the electron diffraction pattern, the fine precipitates are the MX type carbonitride, and consist of Ti, Nb, and Cr elements known from energy dispersive X-ray analysis. The classic definition of the hydrogen embrittlement

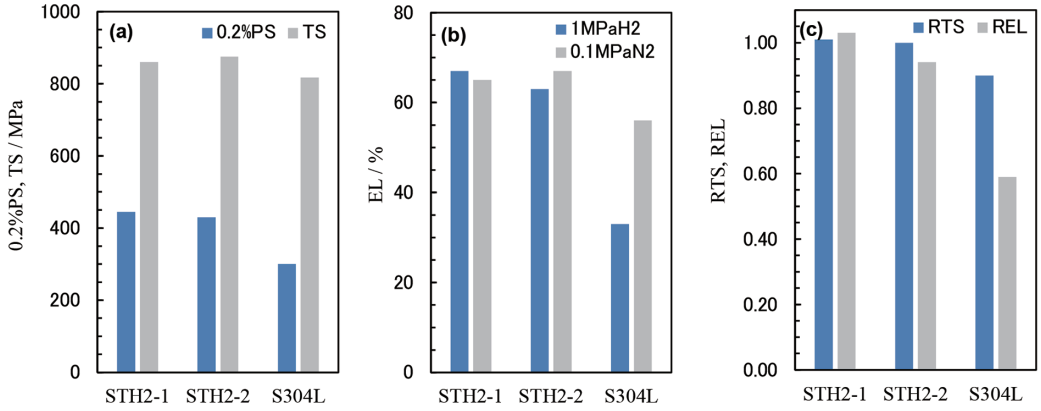

Fig. 11 SSRT properties in gaseous hydrogen of 1 MPa at −40°C
(a) 0.2% PS and tensile strength in 1 MPa H_2 (b) Elongation in 1 MPa H_2 and 0.1 MPa N_2 (c) Relative tensile strength and elongation

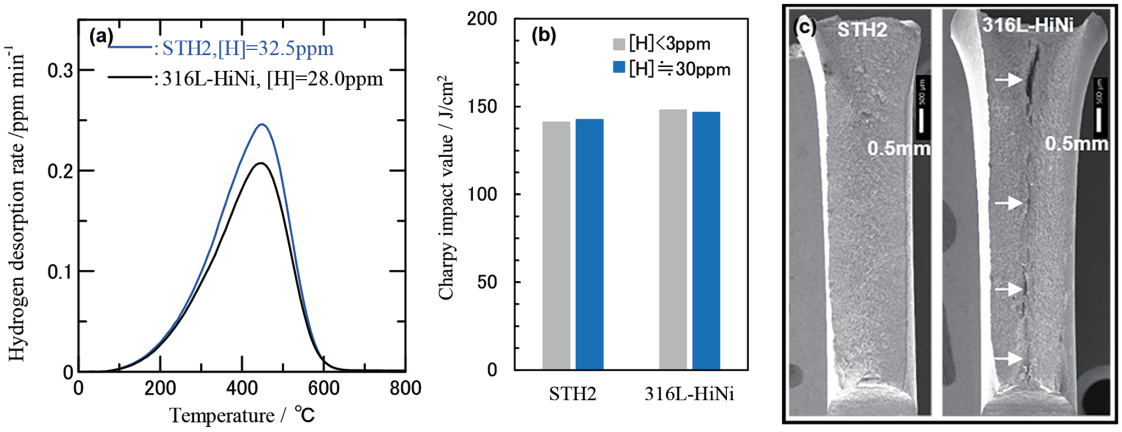

Fig. 12 Effect of hydrogen precharging on cryo-fracture properties
(a) TDA profiles of hydrogen charging specimens (b) Charpy impact value at −196°C (c) SEM observation results of fracture surface

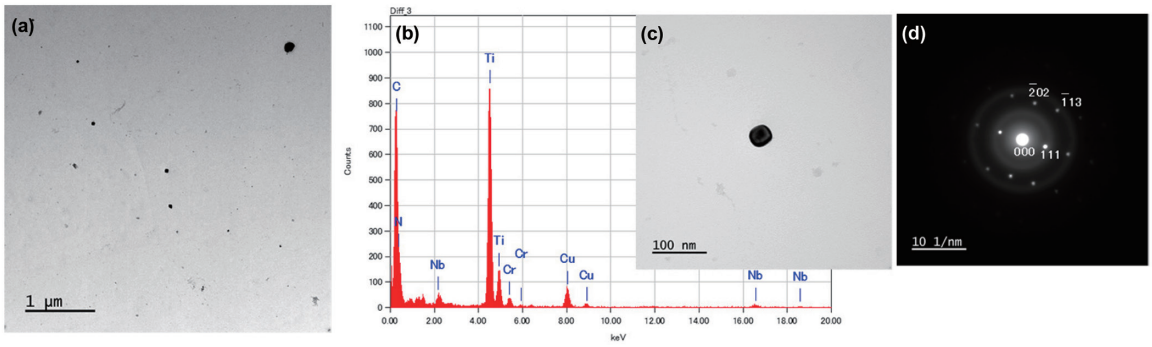

Fig. 13 Analysis results of replica TEM from the thickness center of 316L-HiNi heat-treated at 300°C for 96 h
(a) TEM image of precipitates (b) EDX elemental analysis of the precipitate (c) Analyzed precipitate (d) Electron diffraction pattern from the precipitate

mechanism is that embrittlement is due to the hydrogen-assisted cracks caused by hydrogen being enriched at the stress-concentrated areas,[18] and there is another example of reporting at −196°C at which temperature hydrogen does not diffuse.[19] The internal cracks that occurred in 316L-HiNi in this experiment are considered to be the hydrogen-assisted cracks caused as a result of hydrogen trapped in the MX type carbonitride precipitated by the heat treatment of 300°C × 96 h deteriorating by the Charpy impact test the boundary strength between the precipitates and the base metal, and thereby promoting the generation and development of cracks (voids) originating at the precipitate.

5. Conclusion

In this paper, as application technologies of STH2 thick steel plate to liquid hydrogen use, the result of the evaluation of the properties of TIG welded joints, fracture resistance properties, and the hydrogen embrittlement resistance properties at low temperatures have been summarized.

TIG welded joints using STH2 filler metal exhibit in liquid hydrogen (−253°C) 0.2%PS about double that of SUS316L, and high Charpy absorption energy. Prestrained at −196°C and by the Charpy impact test, $\gamma \rightarrow \alpha'$ transformation is suppressed, and excellent fracture resistance properties are exhibited, and the fracture resistance properties are maintained even when 30 ppm hydrogen is absorbed and held inside. The increase of 0.2%PS and TS of STH2 at low temperatures is considered to be based on the change in dislocation microstructure of the γ phase due to deterioration of γ_{SFE}. Furthermore, as a result of suppression of the localization of stress-concentration owing to the excessive development of planar dislocation array, STH2 is presumed to express excellent fracture resistance properties. Hereafter, promotion of the application of STH2 thick steel plate to a liquid hydrogen storage tank is expected to contribute to the reduction of material cost by resource-saving and material thinning, and improvement in welding workability.

References

1) Yamada, T. et al.: Journal of the High Pressure Gas Safety Institute of Japan. 49 (10), 29 (2012)
2) The High Pressure Gas Safety Institute of Japan: General Gas Security Regulation. 2020
3) The Nikkan Kogyo Shimbun, Ltd.: Handbook for Stainless Steels. 3, Edited by Japan Stainless Steel Association, 1995, p.568
4) Hatano, M. et al.: The Journal of Fuel Cell Technology. 12 (4), 70 (2013)
5) Matsumoto, K. et al.: ASME PVP. 97656 (2013)
6) NEDO: Research and Development on Hydrogen Utilization Technology Research and Development. 2018
7) Hatano, M. et al.: Nippon Steel Technical Report. (126), 56 (2021)
8) Tsuchida, N. et al.: Journal of the Japan Institute of Metals and Materials. 72 (9), 769 (2008)
9) Hatano, M. et al.: Transactions of Society of Automotive Engineers of Japan. 54 (5), 826 (2023)
10) Kimura, M. et al.: Journal of High Pressure Institute of Japan. 60 (1), 24 (2022)
11) NEDO: Establishment of Codes and Standards for Hydrogen Economy Society Guidebook for Effective Utilization of Hydrogen. 2008, p.100
12) Yabumoto, M. et al.: Journal of High Pressure Institute of Japan. 38 (5), 59 (2000)
13) NEDO: International Clean Energy System Technology Utilizing Hydrogen, 1997 Fiscal Year Report on Result of Research. 1998, p.219
14) Fukuyama, S. et al.: Journal of the Japan Institute of Metals and Materials. 67 (9), 456 (2003)
15) Hatano, M. et al.: Phil. Mag. Lett. 99, 404 (2019)
16) Miura, R. et al.: Tetsu-to-Hagané. 73 (6), 131 (1987)
17) Masumura, T. et al.: NETSUSHORI Journal of the Japan Society for Heat Treatment. 59 (4), 222 (2019)
18) Nelson, H.G.: American Society for Testing and Materials. 543, 152 (1972)
19) Harvery, D.P. et al.: J. Mater. Sci. 29, 5485 (1994)

Masaharu HATANO
Dr.Eng., Senior Chief Researcher
New Energy Material Research & Development Div.
Research & Development Center
Nippon Steel Stainless Steel Corporation
3434 Ooaza-shimata, Hikari City, Yamaguchi Pref.
743-8550

Mitsuki SUGEOI
Senior Researcher
New Energy Material Research & Development Div.
Research & Development Center
Nippon Steel Stainless Steel Corporation

Yoichi YAMAMOTO
General Manager
Plate Quality Control Dept.
Yawata Works
Nippon Steel Stainless Steel Corporation

Tatsumi HAMADA
Manager
Plate Quality Control Dept.
Yawata Works
Nippon Steel Stainless Steel Corporation